Magnetoelasticity in $A\mathrm{Cr}_2\mathrm{O}_4$ spinel oxides ($A = $ Mn, Fe, Co, Ni, and Cu)

V. Kocsis,[1] S. Bordács,[1,2] D. Varjas,[1] K. Penc,[3] A. Abouelsayed,[4] C. A. Kuntscher,[4] K. Ohgushi,[5]
Y. Tokura,[2,6,7] and I. Kézsmárki[1]

[1]*Department of Physics, Budapest University of Technology and Economics and Condensed Matter Research Group of the Hungarian Academy of Sciences, 1111 Budapest, Hungary*
[2]*Quantum-Phase Electronics Center, Department of Applied Physics, University of Tokyo, Tokyo 113-8656, Japan*
[3]*Institute for Solid State Physics and Optics, Wigner Research Centre for Physics, Hungarian Academy of Sciences, H-1525 Budapest, Hungary*
[4]*Experimentalphysik 2, Universität Augsburg, D-86135 Augsburg, Germany*
[5]*Institute for Solid State Physics, University of Tokyo, Kashiwa, Chiba 277-8581, Japan*
[6]*Department of Applied Physics, University of Tokyo, Tokyo 113-8656, Japan*
[7]*Cross-correlated Materials Group (CMRG) and Correlated Electron Research Group (CERG), RIKEN Advanced Science Institute, Wako 351-0198, Japan*

Dynamical properties of the lattice structure were studied by optical spectroscopy in $A\mathrm{Cr}_2\mathrm{O}_4$ chromium spinel oxide magnetic semiconductors over a broad temperature region of $T = 10$–335 K. The systematic change of the A-site ions ($A = $ Mn, Fe, Co, Ni and Cu) showed that the occupancy of $3d$ orbitals on the A site has strong impact on the lattice dynamics. For compounds with orbital degeneracy ($\mathrm{FeCr}_2\mathrm{O}_4$, $\mathrm{NiCr}_2\mathrm{O}_4$, and $\mathrm{CuCr}_2\mathrm{O}_4$), clear splitting of infrared-active phonon modes and/or activation of silent vibrational modes have been observed upon the Jahn-Teller transition and at the onset of the subsequent long-range magnetic order. Although $\mathrm{MnCr}_2\mathrm{O}_4$ and $\mathrm{CoCr}_2\mathrm{O}_4$ show multiferroic and magnetoelectric character, no considerable magnetoelasticity was found in spinel compounds without orbital degeneracy as they closely preserve the high-temperature cubic spinel structure even in their magnetic ground state. Aside from lattice vibrations, intra-atomic $3d$-$3d$ transitions of the A^{2+} ions were also investigated to determine the crystal field and Racah parameters and the strength of the spin-orbit coupling.

I. INTRODUCTION

The effect of spin ordering on the symmetry and lattice parameters of magnetic crystals, termed magnetoelasticity, has recently attracted remarkable interest in multiferroic materials and complex magnets. This is because magnetoelasticity is closely related to the magnetocapacitance and other magnetoelectric phenomena.[1–3] The dynamical coupling between lattice vibrations and spin-wave excitations also plays a crucial role in the electromagnon excitations of manganese oxides.[4–6] For several chromium spinel oxides, the materials in the focus of this study, multiferroic ordering has been reported at low temperatures and large magnetic field induced changes were also found in their dielectric response.[1,7–10] In order to reveal the nature and origin of spin-phonon coupling governing magnetoelasticity, optical probe of lattice vibrations has been shown to be an efficient tool for a broad class of chromium spinel oxides and chalcogenides with nonmagnetic A-site ions.[11–14]

At high temperatures, $A\mathrm{Cr}_2\mathrm{O}_4$ chromium spinel oxides have the normal cubic spinel structure corresponding to the space group of $Fd\bar{3}m$ as shown in Fig. 1(a). Within this structure, A^{2+} ions form a diamond lattice with tetrahedral oxygen environment, while magnetic Cr^{3+} ions surrounded by octahedral oxygen cages form a pyrochlore sublattice. In the local crystal field of oxygen ions, the $3d$ orbitals of a Cr^{3+} ion are split into a low-lying t_{2g} triplet and a higher-energy e_g doublet, while the orbitals of an A^{2+} ion are split into a lower e doublet and a higher t_2 triplet as illustrated in Fig. 1(b). The presence of magnetic moment and orbital degeneracy on the A-site ions can change the magnetic and structural properties

in chromium spinel oxides in an additional way as compared to those members of the $A\mathrm{Cr}_2\mathrm{O}_4$ family where Cr^{3+} is the only magnetic ion.

First, the antiferromagnetic $J_{\mathrm{Cr\text{-}Cr}}$ exchange interaction between neighboring Cr^{3+} ions leads to a highly frustrated ground state on the pyrochlore sublattice. This frustration can only be released by the so-called spin-Jahn-Teller effect for compounds with nonmagnetic A-site ions, where lattice distortions induce differences between the exchange coefficients originally uniform for each Cr^{3+}-Cr^{3+} pair. This removes the spin degeneracy of the ground state and consequently a long-range magnetic order can develop as observed at low temperatures in the case of $\mathrm{ZnCr}_2\mathrm{O}_4$ (Refs. 11 and 12) and $\mathrm{CdCr}_2\mathrm{O}_4$ (Ref. 13). In contrast, if A-site ions are magnetic, the coupling of $S = \frac{3}{2}$ Cr^{3+} spins to the A-site spins on the bipartite diamond lattice removes the magnetic frustration, and the magnetic ordering occurs at much higher temperatures comparable to the energy scale of the exchange interactions.

Second, if A-site ions have orbital degeneracy in the cubic spinel structure, it is lifted by a cooperative Jahn-Teller distortion, resulting in a tetragonal structure with space group $I4_1/amd$ even above the magnetic transition temperatures;[15–18] the onset of magnetic order may lead to further reduction of the lattice symmetry through a spin-lattice coupling. On the other hand, chromium oxide spinels with magnetic A sites but without orbital degeneracy are reported to maintain the nearly cubic structure even in their low-temperature magnetic state.[7,19,20] Aside from spinel chromites, the impact of orbital degeneracy on the magnetic and structural properties is clearly manifested in vanadium oxide spinels,
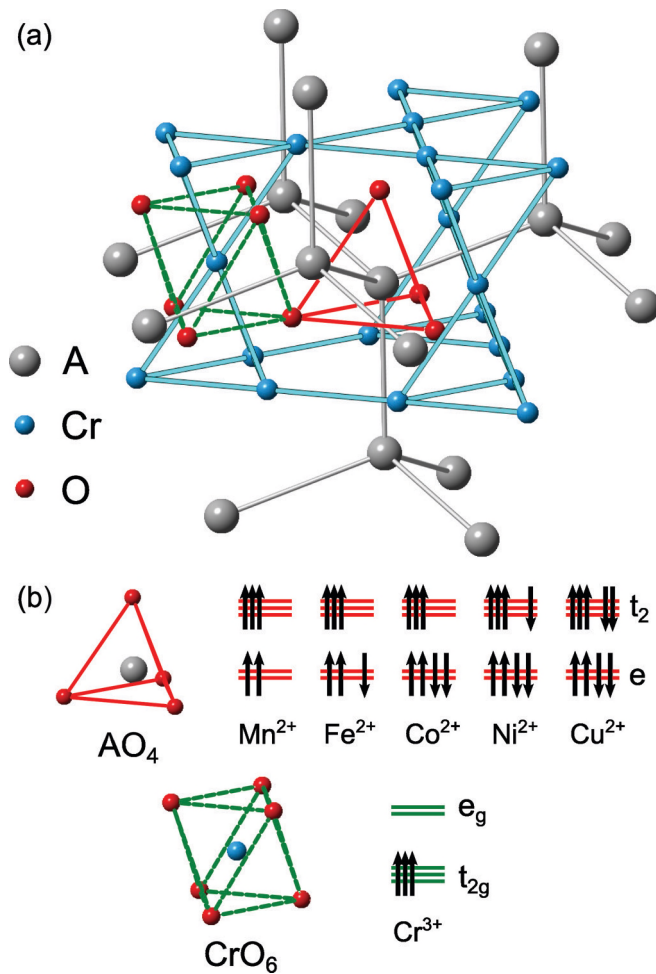
FIG. 1. (Color online) (a) In the structure of ACr_2O_4 spinels, the Cr^{3+} ions (light blue spheres) and the A^{2+} ions (gray spheres) are located on a pyrochlore and a diamond lattice, respectively. The oxygens (red spheres) form octahedral environment around Cr^{3+} ions, while A^{2+} ions are surrounded by tetrahedral oxygen cages. (b) Electron configuration of Cr^{3+} ion and A-site ions with increasing electron number on the $3d$ shell. Here, the splitting due to the local crystal field of the ions in the cubic phase and the effect of Hund coupling are only taken into account.

where both diamond and pyrochlore sublattices can host orbital degeneracy. The most peculiar example is FeV_2O_4,[21] which exhibits successive structural transitions due to the interplay between the Jahn-Teller effect on the two sublattices and the influence of the spin order.

In this paper, we perform a systematic optical study of ACr_2O_4 chromium spinels having magnetic ions also on the A site (A = Mn, Fe, Co, Ni, and Cu). In sequence of the A-site ions, A = Fe, Ni, and Cu compounds are Jahn-Teller active ions with orbital degeneracy, while $MnCr_2O_4$ and $CoCr_2O_4$ spinels have no orbital degrees of freedom [see Fig. 1(b)]. Our main purpose is to reveal the key parameters responsible for the lowering of the lattice symmetry associated with their magnetic ordering, i.e., the origin of magnetoelasticity in these compounds, by an infrared optical study of their lattice dynamics. We also investigate the intra-atomic $3d$-$3d$ transitions of the A-site ions to reveal their electronic states.

Kaplan and Menyuk[22] proposed that for $J_{A\text{-}Cr}$ (exchange coupling between spins of neighboring A^{2+} and Cr^{3+} ions) sufficiently strong relative to $J_{Cr\text{-}Cr}$, the magnetic ground state becomes unique and noncollinear magnetic orders with three different magnetic sublattices can develop. This has been verified experimentally for all these compounds. $CoCr_2O_4$ exhibits ferrimagnetic order below $T_C = 93$ K and an incommensurate conical spin order develops below $T_S = 27$ K, which becomes commensurate with the lattice periodicity at $T_{\text{lock-in}} = 13$ K.[7,23–26] In the conical magnetic phase, the presence of spontaneous electric polarization and ferrotoroidicity were reported.[7] In $MnCr_2O_4$, the ferrimagnetic transition occurs at $T_C = 48$ K, while the onset of the long-range conical order takes place at $T_S = 14$ K.[19,25,26] Similarly, $FeCr_2O_4$ becomes a ferrimagnet below $T_C = 93$ K and the conical order sets in at $T_S = 35$ K.[26–29] Ferroelectric polarization was observed in this material below T_C.[10] The magnetic structures of $NiCr_2O_4$ and $CuCr_2O_4$ are rather different from the former compounds. According to magnetization measurements, $NiCr_2O_4$ becomes a collinear ferrimagnet at $T_C = 74$ K, where the simultaneous lowering of the lattice symmetry to orthorhombic was verified by x-ray scattering measurements.[30] Below $T_S = 31$ K, this compound exhibits a Yafet-Kittel-type canted ferrimagnetic order.[31] In $CuCr_2O_4$, the Yafet-Kittel-type magnetic order emerges right from the paramagnetic state at $T_C = 152$ K.[26,32]

II. EXPERIMENTAL TECHNIQUES AND DATA ANALYSIS

Single crystals of ACr_2O_4 for A = Mn, Fe, Co with typical linear dimensions of 300–600 μm were grown by chemical vapor transport, while $CuCr_2O_4$ was prepared by the flux decomposition method as described elsewhere.[26] We adopted the flux method of Wanklyn *et al.*[33] using solely PbO flux in order to grow $NiCr_2O_4$.

Unpolarized normal incidence reflectivity spectra were studied on the (111) surface for A = Mn, Fe, Co, Ni and on the (010) surface of $CuCr_2O_4$ over the temperature range of T = 10–335 K with a Bruker IFS 66v/s Fourier-transform IR spectrometer coupled to a microscope (Bruker Hyperion). The samples were mounted on the cold unit of a Konti-Cryostat-Mikro optical cryostat manufactured by CryoVac. The temperature was precisely monitored using thermometers located in the close vicinity of the samples. The lattice vibrations were found to be sensitive to polishing induced mechanical strain, thus, reflectivity spectra were measured on as-grown surfaces at low energies, ω = 100–7700 cm^{-1}. Due to surface roughness of $MnCr_2O_4$ and $NiCr_2O_4$ samples, we had to use polished surfaces to avoid light scattering at higher energies. Correspondingly, reflectivity spectra were also recorded over ω = 1700–24 000 cm^{-1} on polished surfaces. The reflectivity spectrum of each compound was measured up to ω = 250 000 cm^{-1} at room temperature with use of synchrotron radiation at UVSOR Institute for Molecular Science, Okazaki, Japan.[26,34]

Optical conductivity spectra were obtained from the reflectivity data by Kramers-Kronig transformation. The low-energy part of the measured reflectivity spectra was extrapolated to zero photon energy as a constant value, while the high-energy part was assumed to follow the free-electron model above ω = 1 000 000 cm^{-1}. The advantage of the optical conductivity
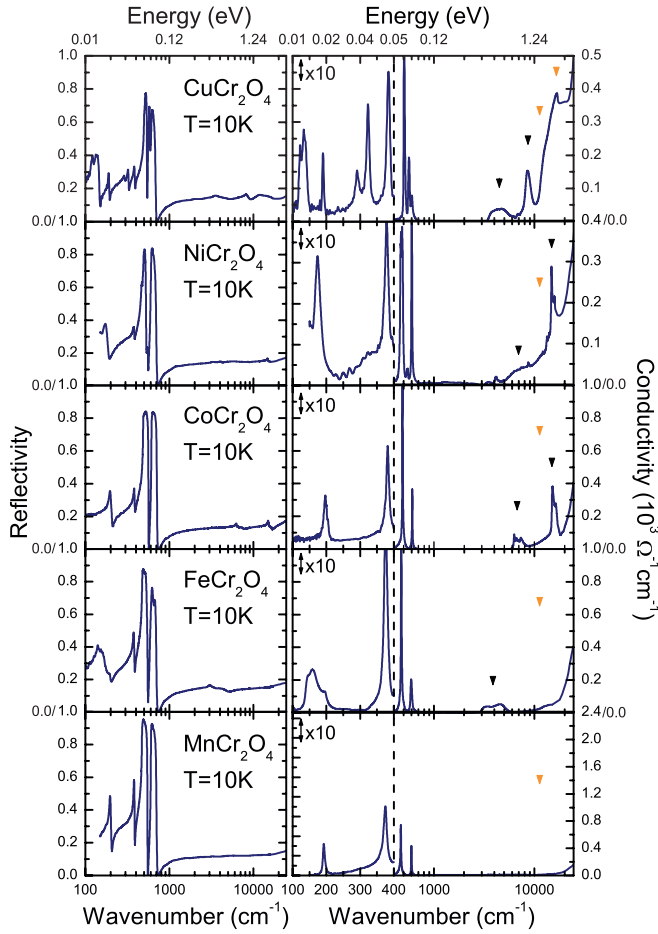
FIG. 2. (Color online) Reflectivity spectra (left panel) and the real part of the optical conductivity spectra (right panel) over the photon energy range of 100 cm^{-1} and 24 500 cm^{-1} for the ACr$_2$O$_4$ (A = Mn, Fe, Co, Ni, and Cu) spinel crystals measured at T = 10 K. This spectral range covers the in-gap excitations, namely, the optical phonon modes and the intra-atomic $3d$-$3d$ transitions. The $3d$-$3d$ transitions of A^{2+} ions are indicated by black triangles, while the $3d$-$3d$ transitions of Cr^{3+} ions are shown with orange triangles. The low-energy part of the conductivity spectra is 10 times magnified for better visibility. In MnCr$_2$O$_4$ and CoCr$_2$O$_4$, only the four T_{1u}(IR) infrared active phonon modes corresponding to the cubic symmetry are visible. In the other compounds, some of these four modes are clearly split indicating the lowering of the crystal symmetry.

spectra versus the reflectivity spectra is that phonon excitations appear as sharp peaks in the former, while close resonances are more difficult to resolve in the reflectivity data. In the analysis of the optical phonon modes, we fitted the corresponding low-energy part of the optical conductivity spectra with a sum of Lorentzian peaks according to

$$\sigma(\omega) = -i\omega\varepsilon_o \left(\varepsilon_\infty - 1 + \sum_{i=1} \frac{S_i}{\omega_i^2 - \omega^2 - i\gamma_i\omega} \right), \qquad (1)$$

where S_i, ω_i, and γ_i stand for the oscillator strength, the resonance frequency, and the damping rate of the modes, ε_o is the vacuum permittivity, and ε_∞ is the dielectric constant at high energies.

III. RESULTS

The measured reflectivity and the corresponding optical conductivity spectra are plotted on common energy scales for ACr$_2$O$_4$ spinels (A = Mn, Fe, Co, Ni, and Cu) in Fig. 2 at T = 10 K. At the high-energy side, the upturn of the optical conductivity corresponds to a band gap of $\Delta \approx 2.5$ eV characteristic to these chromium spinel oxides. The gap value is not significantly influenced by the variation of the A-site ions, therefore, the lowest-energy interband transition is mainly related to the O $2p \rightarrow$ Cr $3d$ charge transfer excitations. Below the optical gap, weak excitations exist in the visible and near-infrared regions. Since these structures are sensitive to the change of the A-site ion, they are assigned to intra-atomic $3d$-$3d$ transitions of the tetrahedrally coordinated A cations (black triangles in Fig. 2) in agreement with former optical studies.[26] A broad and low-intensity hump at $E = 1.6$ eV is the only structure common in each spectra (orange triangles in Fig. 2). This feature is due to the $3d$-$3d$ transitions of the Cr^{3+} ions. Finally, in the low-energy range ($\omega = 100$–700 cm^{-1}), optical phonon excitations characteristic to the lattice structure are observed. In the following sections, the dependence of the phonon excitations and the $3d$-$3d$ transitions on the A-site cations and the temperature are discussed.

A. Lattice vibrations in ACr$_2$O$_4$ spinels without orbital degree of freedom

According to powder x-ray diffraction measurements, the lattice symmetry for A = Mn, Fe, Co belongs to the cubic space group $Fd\bar{3}m$ at room temperature, while in the case of A = Ni, Cu, the symmetry is already tetragonal with the space group $I4_1/amd$.[17,26]

The factor group analysis for cubic spinels [$Fd\bar{3}m$ space group, $m3m$ (O$_h$) point group] yields 16 optical phonon modes at the Γ point:

$$\Gamma(A\text{Cr}_2\text{O}_4)_{Fd\bar{3}m} = A_{1g}(\text{R}) \oplus 2A_{2u}(\text{S}) \oplus E_g(\text{R})$$
$$\oplus 2E_u(\text{S}) \oplus T_{1g}(\text{S}) \oplus 4T_{1u}(\text{IR})$$
$$\oplus 3T_{2g}(\text{R}) \oplus 2T_{2u}(\text{S}), \qquad (2)$$

where abbreviations IR, R, and S refer to infrared-active, Raman-active, and silent modes, respectively. Thus, in the
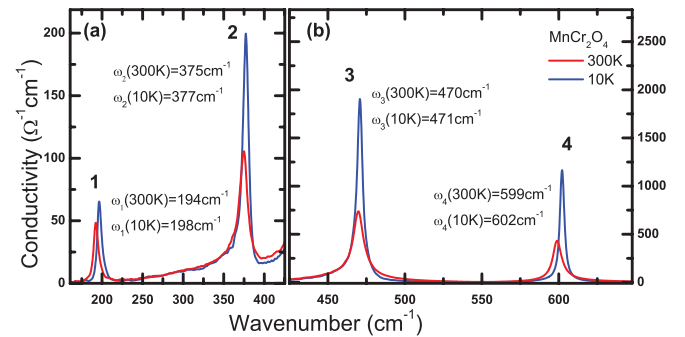

FIG. 3. (Color online) Optical conductivity spectra of MnCr$_2$O$_4$ at T = 300 and 10 K contain four distinct phonon modes. Neither the ferrimagnetic transition at T_C = 51 K nor the onset of conical spin order at T_S = 14 K are accompanied with an observable splitting of these T_{1u}(IR) phonon modes. Note that the conductivity scales for panels (a) and (b) differ by more than an order of magnitude.
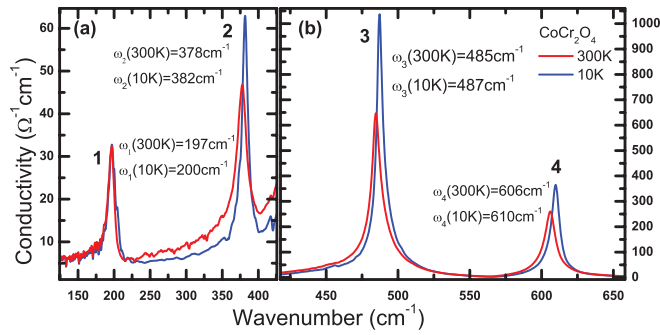
FIG. 4. (Color online) Optical conductivity spectra of CoCr$_2$O$_4$ at $T = 300$ and 10 K. Similarly to MnCr$_2$O$_4$, no splitting of the four T_{1u}(IR) phonon modes can be traced either below the ferrimagnetic transition at $T_C = 93$ K or upon the conical spin ordering at $T_S = 26$ K.

cubic phase, four T_{1u}(IR) modes are expected to appear in the optical spectra, all of which have threefold degeneracy. When the lattice symmetry is reduced to tetragonal, each of these T_{1u} lattice vibrations is split into an A_{2u}(IR) singlet and an E_u(IR) doublet mode. Furthermore, the two originally silent T_{2u} phonon modes can split into an infrared-active E_u(IR) doublet and a silent B_{2u} singlet. If the symmetry of the lattice is further lowered, the degeneracy of each mode is completely lifted.

Optical conductivity spectra of MnCr$_2$O$_4$ and CoCr$_2$O$_4$, spinels with no orbital degrees of freedom, are shown in Figs. 3 and 4, respectively. All the four infrared-active

T_{1u}(IR) optical phonon modes expected in the cubic phase are observed at room temperature for the both compounds. As the temperature is decreased to $T = 10$ K, the spectral width of each phonon mode is reduced by ~30%. The detailed temperature dependence of the resonance frequencies was determined by fitting the spectra according to Eq. (1) and the results are summarized in Fig. 5.

All the modes show weak hardening toward lower temperatures followed by a tiny softening upon the ferrimagnetic transition. In MnCr$_2$O$_4$, the first and second modes (located at ~195 cm^{-1} and ~376 cm^{-1}, respectively) are shifted toward higher energies upon the conical spin ordering at $T_S = 14$ K. In CoCr$_2$O$_4$, an anomalous broadening was observed for the third and fourth modes below $T_C = 93$ K. However, no clear sign of phonon splitting can be discerned in either of the two compounds within the resolution of our experiment, ~0.5 cm^{-1}. These results are compatible with a very weak, if any, distortion of the cubic lattice in MnCr$_2$O$_4$ and CoCr$_2$O$_4$ even at $T = 10$ K.

B. Phonon modes in ACr$_2$O$_4$ spinels with Jahn-Teller active ions

In FeCr$_2$O$_4$ and NiCr$_2$O$_4$ spinel oxides with Jahn-Teller active A^{2+} ions, the presence of four T_{1u}(IR) phonon modes are observed above room temperature (Figs. 6 and 7), indicating the stability of the high-symmetry cubic spinel structure. Upon the Jahn-Teller transition of FeCr$_2$O$_4$ at $T_{JT} = 135$ K, however, the lowest- and the highest-energy modes, while in
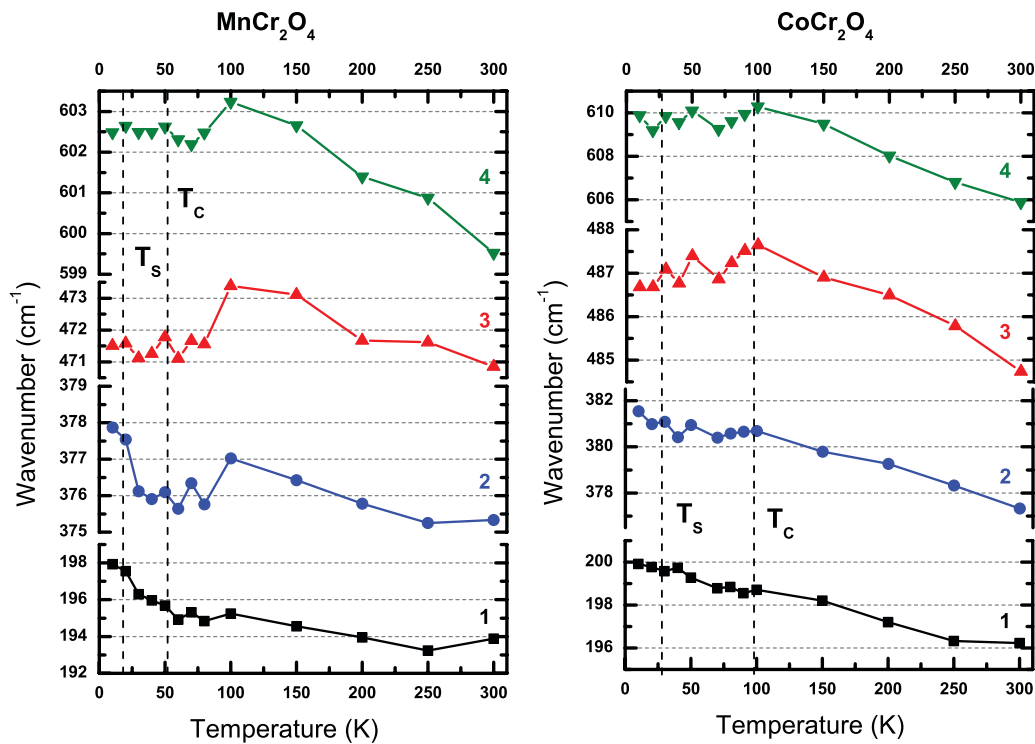

FIG. 5. (Color online) Temperature dependence of phonon mode energies in MnCr$_2$O$_4$ and CoCr$_2$O$_4$. Mn^{2+} and Co^{2+} ions, located on the A site of the spinel structure, have no orbital degeneracy [Fig. 1(b)]. Correspondingly, no structural transition associated with a cooperative Jahn-Teller distortion has been observed. No measurable splitting of the phonon modes occurs upon the magnetic phase transitions either. T_C and T_S label the transition to a ferrimagnetic state and to the ground state with conical spin order, respectively.
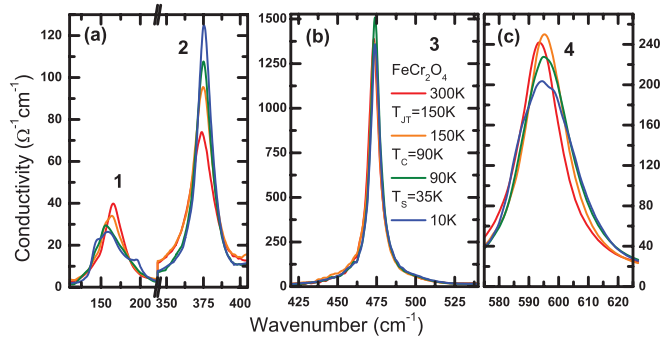
FIG. 6. (Color online) Optical conductivity spectra of FeCr$_2$O$_4$ at various temperatures in the vicinity of the Jahn-Teller transition at $T_{JT} = 135$ K, the ferrimagnetic ordering at $T_C = 93$ K, and the onset of the conical order at $T_S = 35$ K. Lowering of the crystal symmetry can be traced as temperature-induced splitting of the lowest- (a) and the highest-energy (b) phonon modes both at T_{JT} and T_C, while splitting of the other two T_{1u}(IR) modes can not be resolved.

NiCr$_2$O$_4$ below $T_{JT} = 320$ K the two high-energy modes are split due to the structural transition to the tetragonal state.

Aside from the splitting of the third and fourth modes in NiCr$_2$O$_4$, a new excitation appears below the Jahn-Teller transition at $\omega_5 = 545$ cm^{-1} [see Fig. 7(c)]. This fifth mode has a low oscillator strength, short lifetime, and can not be deduced from either of the cubic T_{1u}(IR) phonons. However, in the tetragonal phase, the originally silent T_{2u}(S) phonon mode can split into an infrared-active E_u(IR) doublet and a silent B_{2u}(S) singlet beside the splitting of the T_{1u}(IR) modes to A_{2u}(IR) $\oplus$ E_u(IR). We assign this weak mode around $\omega_5 = 545$ cm^{-1} to such an E_u(IR) mode originating from one of the two T_{2u}(S) modes silent in the cubic symmetry. Another mode with similarly small intensity emerges just below T_{JT} in the vicinity of the third T_{1u}(IR) mode. We assign it to the other E_u(IR) mode activated by the tetragonal splitting. The fact that the third T_{1u}(IR) is split into two branches at T_{JT} and becomes three nondegenerate modes with comparable oscillator strengths below T_C may support this assignment.

The optical conductivity spectra of CuCr$_2$O$_4$ are shown in Fig. 8. Each T_{1u}(IR) mode is already split to A_{2u}(IR) $\oplus$ E_u(IR) at room temperature in accordance with its cubic to tetragonal phase transition at $T_{JT} = 854$ K. The remaining twofold degeneracy of each E_u(IR) is lifted upon the ferrimagnetic transition. In contrast to NiCr$_2$O$_4$, no activation of silent modes can be discerned.

The temperature dependence of the phonon frequencies are summarized in Fig. 9 for the spinel oxides with orbital degeneracy $A =$ Fe, Ni, and Cu. The ferrimagnetic phase transition completely removes the threefold degeneracy of some of the cubic T_{1u}(IR) modes in all the three compounds, therefore, the cubic symmetry of the lattice is lower than tetragonal at the ground state of these compounds. The modes whose degeneracy is partly lifted by the Jahn-Teller distortion exhibit further splitting upon the subsequent magnetic transition at T_C except for the highest-energy mode in NiCr$_2$O$_4$. The magnetically induced splitting is as large as $\Delta\omega/\omega \approx 10\%$ for the lower-energy vibrations. The sensitivity of the respective phonon modes to the magnetic ordering depends on the chemical composition; in FeCr$_2$O$_4$, the first and the
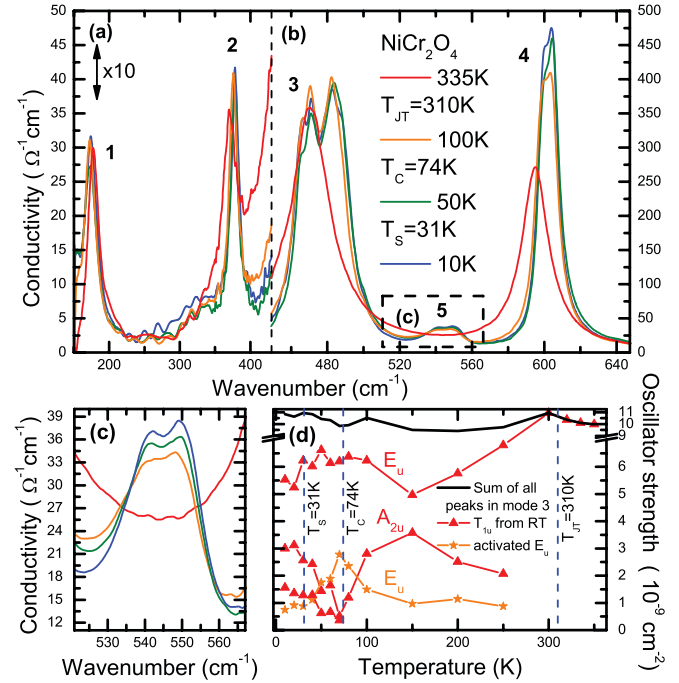

FIG. 7. (Color online) (a), (b) Optical conductivity spectra of NiCr$_2$O$_2$ at various temperatures over the region of the Jahn-Teller transition at $T_{JT} = 320$ K, the ferrimagnetic ordering at $T_C = 74$ K, and the onset of the canted magnetic structure at $T_S = 31$ K. Splitting of the third and the fourth T_{1u}(IR) modes can be observed both at T_{JT} and T_C. Scale of the low-energy part is magnified 10 times larger. (c) Between these modes, the activation of an E_u(IR) mode, which originates from a T_{2u}(S) mode being silent in the cubic phase, can be followed. Rigorous analysis shows the activation of another E_u(IR) mode upon T_{JT}, which is located among the branches of the third T_{1u}(IR) mode. (d) Oscillator strength for this E_u(IR) mode and for the branches of the third T_{1u}(IR) mode as a function of temperature.

fourth modes, in NiCr$_2$O$_4$ the third mode, while in CuCr$_2$O$_4$ all the modes are split. Furthermore, the ferroelectric phase transition in FeCr$_2$O$_4$ is accompanied by a sudden hardening of the lower-energy modes. The partial activation of two silent T_{2u}(S) vibrations was only observed in NiCr$_2$O$_4$. Among these new E_u(IR) modes, the vibration around $\omega_5 = 545$ cm^{-1} is
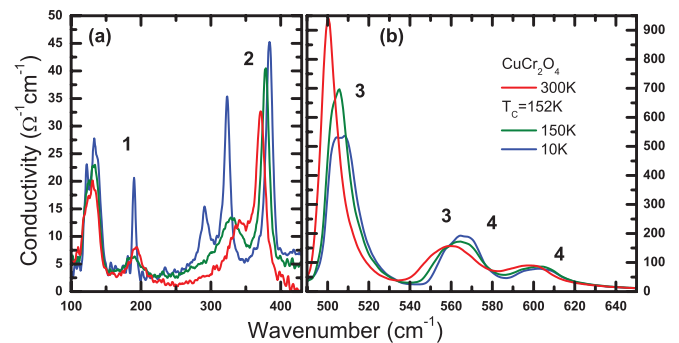

FIG. 8. (Color online) Optical conductivity spectra of CuCr$_2$O$_4$ at various temperatures. At room temperature, all T_{1u}(IR) phonon modes are split due to the Jahn-Teller transition at $T_{JT} = 854$ K. For each mode, the remaining degeneracy is lifted upon the magnetic ordering at $T_C = 152$ K.
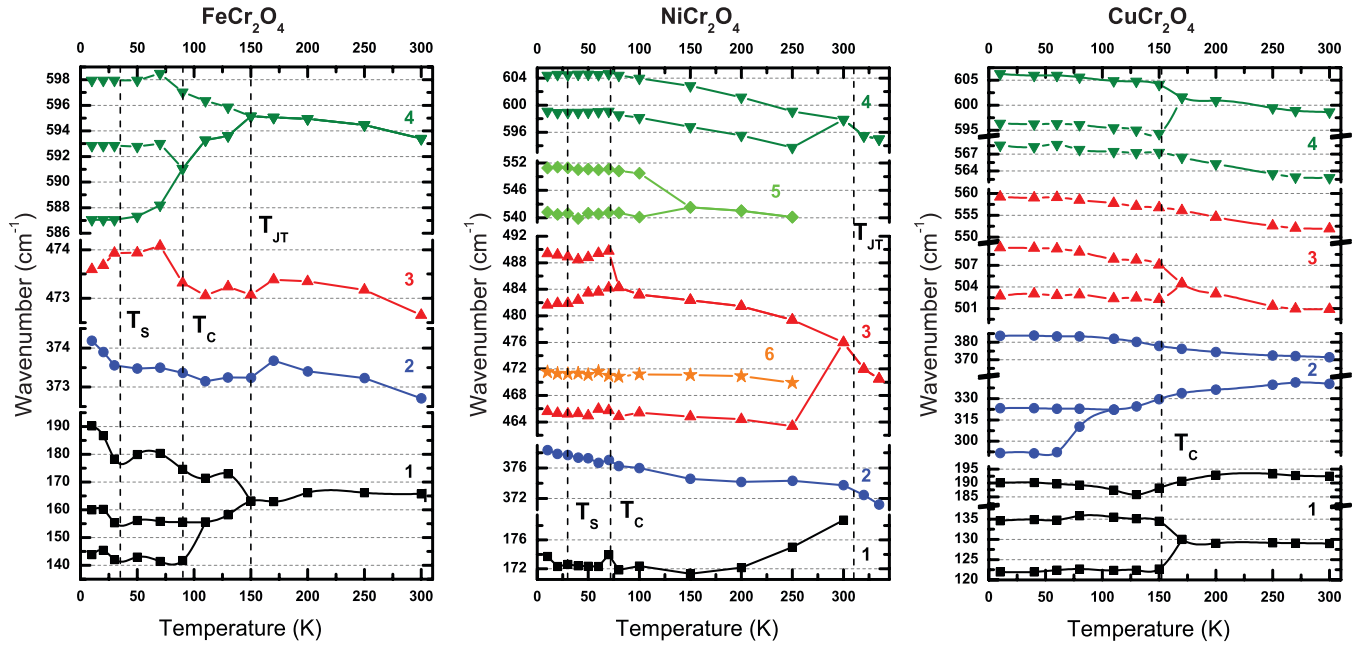
FIG. 9. (Color online) Temperature dependence of phonon energies in $FeCr_2O_4$, $NiCr_2O_4$, and $CuCr_2O_4$. Lattice vibrations originating from the same T_{1u} and T_{2u} cubic modes are labeled with the same color and symbol. The temperature of the phase transitions are indicated by dashed lines.

sensitive to the magnetic ordering as it shows a splitting in the vicinity of T_C. As already reported in literature,[35] the lowest-energy mode in this compound exhibits an anomalous softening with decreasing temperature. Such unusual temperature dependence of the low-energy vibrations was also found in FeV_2O_4.[35]

C. Intra-3*d*-band excitations of *A*-site ions

Weak in-gap excitations observed over the mid-infrared–visible range in ACr_2O_4 spinels are interpreted as transitions within the 3*d* levels of the *A*-site cations split by the local crystal field, the Coulomb interaction, and the spin-orbit coupling.[26] In ACr_2O_4 compounds, these parity-forbidden transitions become allowed due to the lack of inversion symmetry for the tetrahedrally coordinated *A*-site ions. This provides the possibility to investigate the electronic structure of the *A*-site ions by optical spectroscopy. In the subsequent section, the optical conductivity spectra are analyzed in terms of the ligand field theory.

We observed 3*d*-3*d* excitations in the optical conductivity spectra of *A* = Cu, Ni, Co and *A* = Fe chromium spinel oxides, while no such transition was found in $MnCr_2O_4$ (see Fig. 2). The absence of this excitation in the latter compound indicates that high-spin state is realized for the *A*-site ions due to strong Hund coupling [as shown in Fig. 1(b)] since 3*d*-3*d* transitions become spin forbidden within the half-filled *d* band of the Mn^{2+} ion.

Ohgushi *et al.* have discussed the case of *A* = Fe and Co in the frame of the ligand field theory including spin-orbit coupling.[26] The main results of their calculations are reproduced in the first two panels of Fig. 10. The transition in $FeCr_2O_4$ at around ~0.49 eV was assigned as a single-electron transition through the crystal-field gap $^5E(e^3t_2^3) \rightarrow {}^5T_2(e^2t_2^4)$,

while the two absorbtion peaks in $CoCr_2O_4$ at around ~0.84 and ~1.95 eV correspond to the $^4A_2(e^4t_2^3) \rightarrow {}^4T_2(e^3t_2^4)$ and $^4A_2(e^4t_2^3) \rightarrow {}^5T_1(e^3t_2^4)$ transitions, respectively. From these excitations, the crystal-field splitting corresponding to the cubic state and the Racah parameter B, characteristic to the Coulomb interaction, can be determined. The values obtained for Co^{2+} are $\Delta E = 0.84$ eV and $B = 0.093$ eV, while for Fe^{2+}, $\Delta E = 0.49$ eV has been reported.[26]

In the low-temperature optical conductivity spectrum of $NiCr_2O_4$, two distinct structures are visible around ~0.95 and ~1.94 eV, which can be assigned as 3*d*-3*d* transitions of the tetrahedrally coordinated Ni^{2+}. Since the fine structure of these peaks can not be resolved, cubic (T_d) site symmetry was assumed in our model and the tetragonal distortion was neglected.[36] The energy levels of the eight 3*d* electrons of the Ni^{2+}, relevant for the single-particle excitations, is depicted in Fig. 10(c). The two peaks in the optical conductivity spectrum were fitted with two Lorentzian corresponding to the two electric-dipole-allowed transitions: $^3T_1(e^4t_2^4) \rightarrow {}^3T_2(e^3t_2^5)$ and $^3T_1(e^4t_2^4) \rightarrow {}^3T_1(e^3t_2^5)$ [see Fig. 11(a)]. The cubic crystal-field splitting and the Racah parameter for the Ni^{2+} ion deduced from the transition energies are $\Delta E = 1.20$ eV and $B = 0.082$ eV, respectively. The spin-orbit and the unresolved tetragonal splitting may be responsible for the large width of the resonances peaks.

In contrast to $NiCr_2O_4$, the crystal lattice of $CuCr_2O_4$ has strong tetragonal distortion at low temperature.[17] Perhaps, the low symmetry of the lattice is responsible for the large number of peaks observed in the near-infrared and visible parts of the optical conductivity spectrum. As in other ACr_2O_4 compounds, the excitations around $E = 1.6$ eV are assigned to the intra-atomic 3*d*-3*d* transitions of Cr^{3+} split by the tetragonal distortion. Compared to the sister compounds, the strength of this transition is remarkably enhanced. The two
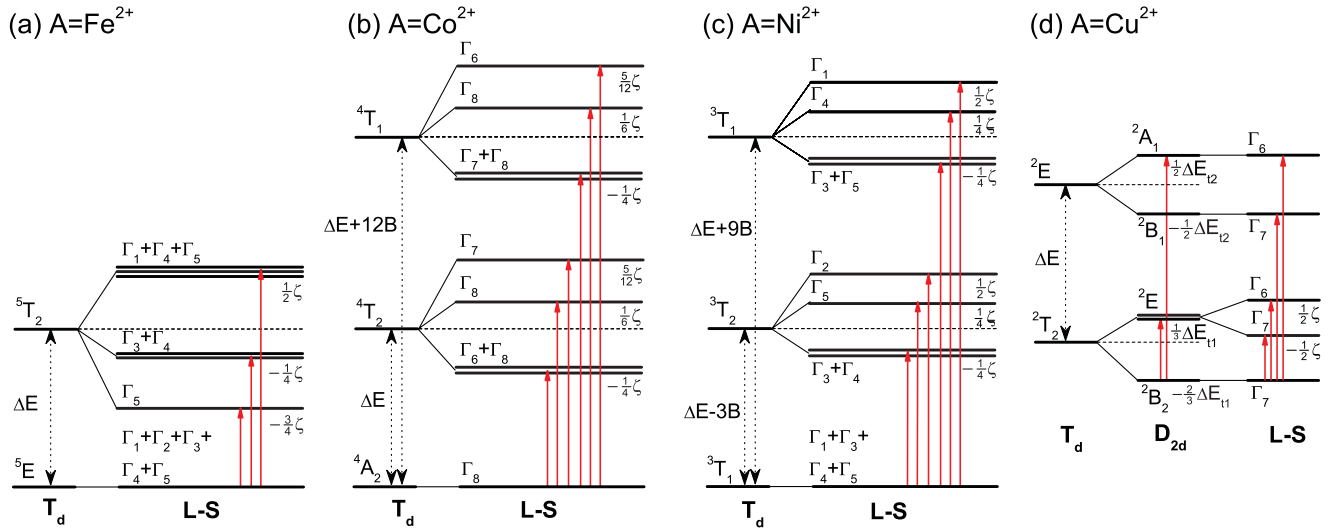
FIG. 10. (Color online) Energy-level diagrams corresponding to Fe^{2+}, Co^{2+}, Ni^{2+}, and Cu^{2+} $3d$ orbitals occupied by holes. In these diagrams, only the spin-allowed single-particle excitations are shown, red arrows represent the allowed optical transitions. (a), (b) $3d$-$3d$ optical transitions within the d band of the A-site ion split by the cubic (T_d) crystal field ΔE, the Racah parameter B, and the spin-orbit interaction ζ for A = Fe^{2+} and A = Co^{2+} (Refs. 26 and 36). (c) In the case of A = Ni^{2+}, the effect of local T_d symmetry and spin-orbit interaction was taken into account, the latter as the weakest perturbation. Here, symmetry lowering associated with the weak tetragonal splitting was neglected. (d) In the case of A = Cu^{2+}, the effect of Jahn-Teller distortion, i.e., tetragonal splitting, ΔE_1 was considered stronger than the spin-orbit interaction.

lower-energy peaks at around $\sim$0.56 and $\sim$1.06 eV are related to the $3d$-$3d$ transitions of Cu^{2+}. Due to the strong Jahn-Teller distortion, we assumed tetragonal D_{2d} local symmetry in the ligand field calculation and the spin-orbit coupling was also

taken into account. The energy levels and the possible optical transitions are shown in Fig. 10(d). In D_{2d} symmetry, the $^2B_2 \rightarrow {}^2B_1$ transition is forbidden, and only the spin-orbit interaction makes it weakly allowed, therefore, its oscillator strength was assumed to be zero. The optical conductivity spectrum was fitted with three Lorentzian oscillators as shown in Fig. 11(b). The obtained values for the cubic and the tetragonal crystal-field splitting and the spin-orbit coupling are $\Delta E = 0.69$ eV, $\Delta E_{t1} = 0.56$ eV, and $\zeta = 0.1$ eV, respectively, if the ΔE_{t2} tetragonal splitting within the cubic ^2E term is neglected.

The different parameters of the electronic structure of the A-site ions, namely, the cubic and tetragonal crystal-field splittings ΔE and ΔE_t, respectively, the Racah parameter B and the strength of the spin-orbit coupling ζ are summarized in Table I for the investigated ACr$_2$O$_4$ spinel oxides. These fundamental energy scales may serve as a starting point for a microscopic theory describing the magnetoelasticity of the ACr$_2$O$_4$ spinels and provide in general an important input to theories describing their magnetic states.
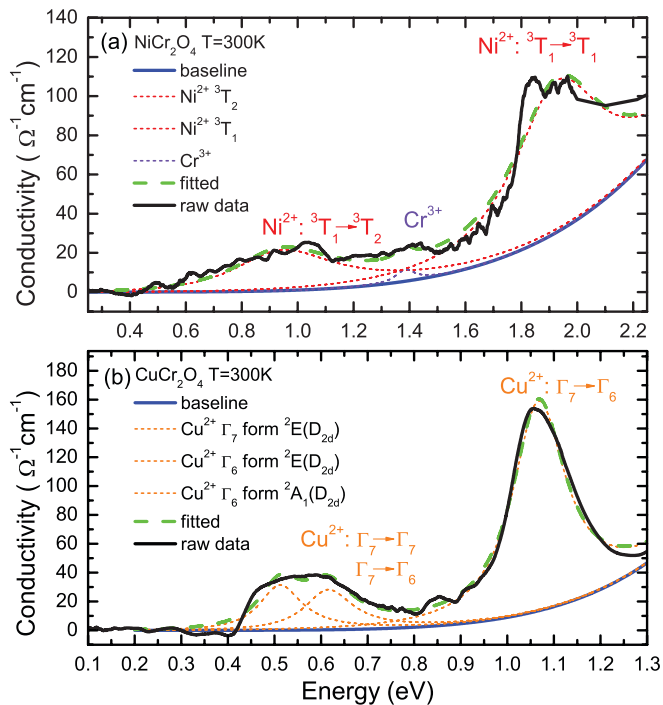

FIG. 11. (Color online) Analysis of the intra-atomic $3d$-$3d$ transitions in NiCr$_2$O$_4$ and CuCr$_2$O$_4$ as shown in panels (a) and (b), respectively. Labels correspond to notation introduced in Fig. 10. Aside from the oscillators, there is a common baseline corresponding to the tail of the band edge.

TABLE I. Cubic (ΔE) and tetragonal (ΔE_t) crystal-field splittings, the Racah parameter (B), and the strength of the spin-orbit coupling (ζ) as determined in this study for various spinel oxides with magnetic A-site ions. The values formerly reported in Ref. 26 for Fe^{2+} and Co^{2+} are closely reproduced in this study.

	Fe^{2+}[26]	Co^{2+}[26]	Ni^{2+}	Cu^{2+}
ΔE (eV)	0.49	0.84	1.20	0.69
$\Delta E_{t1}, \Delta E_{t2}$ (eV)				0.56, $\sim$0
B (eV)		0.093	0.082	
ζ (eV)	0.13 ($^5T_2$)	0.25 ($^4T_2$)		0.1 ($^2T_2$)
		0.34 ($^4T_1$)		

IV. DISCUSSION

From the viewpoint of the dynamical properties of the lattice, ACr_2O_4 chromium spinels (A = Mn, Fe, Co, Ni, and Cu) can be classified into two distinct groups. The main results of our optical study about these classes are summarized in Figs. 5 and 9.

In the first group, the A-site ions have no orbital degeneracy (A = Mn and Co) and neither of these compounds show observable phonon mode splitting upon the magnetic phase transitions from room temperature down to $T = 10$ K. Anomalous broadening of the third and fourth modes of $CoCr_2O_4$ below $T_C = 93$ K is observed, which may indicate a mode splitting slightly below the spectral resolution of our experiment (~ 0.5 cm^{-1}). In $MnCr_2O_4$, we could not even follow any broadening of the modes associated with the magnetic transitions. Therefore, we conclude that the magnetoelasticity is weak in these compounds and the cubic symmetry of the lattice is nearly preserved even in their magnetically ordered ground state.

For materials in the second class, where A-site ions are Jahn-Teller active, i.e., they have orbital degeneracy in the cubic phase, we observed phonon-mode splittings associated with the cooperative Jahn-Teller distortion. The sequence of the splittings shows that a cubic to tetragonal distortion takes place at T_{JT}. Phonon modes in $CuCr_2O_4$ exhibit a relative splitting of $\approx 30\%$, $\approx 8\%$, $\approx 9\%$, and $\approx 7\%$ in ascending order of phonon energies already at room temperature.[20] For comparison, splitting of the third and fourth phonon modes in $NiCr_2O_4$ is $\approx 4\%$ and $\approx 1\%$, while the lowest- and highest-energy phonons in $FeCr_2O_4$ are split by $\Delta\omega/\omega_o \approx 20\%$ and $\approx 1\%$, respectively. Most of the modes whose degeneracy is partly lifted by the cooperative Jahn-Teller distortion or those activated upon the splitting of silent T_{2u} lattice vibrations, as is the case in $NiCr_2O_4$, are further split upon the ferrimagnetic ordering. The magnitude of the magnetically induced splitting is in the range of $\approx 10\%$ for low-energy and $\approx 1\%$ for high-energy phonon modes. Large splitting of low-energy modes implies strong spin-lattice coupling for these lattice vibrations, resulting in strong magnetoelastic effects. We believe that signatures of magnetoelasticity should also be manifested upon the magnetic phase transitions in the anomalous temperature dependence and the anisotropy of thermal expansion and sound-wave propagation similarly to the case of, e.g., $ZnCr_2S_4$ (Ref. 37) or $CdCr_2O_4$ (Ref. 38). Recently, the static orthorhombic distortion of the crystalline lattice upon the magnetic phase transition has also been observed by means of high-resolution x-ray diffraction in $NiCr_2O_4$ and $CuCr_2O_4$.[30,39]

In conclusion, we found that in ACr_2O_4 spinel compounds, where the frustration of the pyrochlore sublattice is lifted by long-range magnetic ordering due to the exchange interaction between the spins of the A^{2+} and Cr^{3+} ions, the criterion of strong magnetoelasticity is the orbital degeneracy of the A-site ion in the high-symmetry cubic phase. This observation is valid irrespective to the details of the magnetic order, i.e., we found strong magnetoelasticity for the compounds $FeCr_2O_4$, $NiCr_2O_4$, and $CuCr_2O_4$ independently whether they have conical or canted spin order in their ground state. A theoretical model reproducing the effect of orbital occupancy on the magnetoelasticity of these compounds will be published elsewhere.[40] Moreover, based on the analysis of the intra-atomic $3d$-$3d$ transition of the A-site ions, we could determine the following fundamental energies: crystal-field splitting in the cubic and tetragonal phases, the Racah parameters representing the strength of the intraatomic Coulomb repulsion, and the spin-orbit interaction in some cases.

[1] J. Hemberger, P. Lunkenheimer, R. Fichtl, H.-A. Krug von Nidda, V. Tsurkan, and A. Loidl, Nature (London) **434**, 364 (2005).

[2] V. Gnezdilov, P. Lemmens, Yu. G. Pashkevich, Ch. Payen, K. Y. Choi, J. Hemberger, A. Loidl, and V. Tsurkan, Phys. Rev. B **84**, 045106 (2011).

[3] A. B. Harris, T. Yildirim, A. Aharony, and O. Entin-Wohlman, Phys. Rev. B **73**, 184433 (2006).

[4] Y. Takahashi, N. Kida, Y. Yamasaki, J. Fujioka, T. Arima, R. Shimano, S. Miyahara, M. Mochizuki, N. Furukawa, and Y. Tokura, Phys. Rev. Lett. **101**, 187201 (2008).

[5] M. Mochizuki, N. Furukawa, and N. Nagaosa, Phys. Rev. Lett. **105**, 037205 (2010).

[6] M. Mochizuki, N. Furukawa, and N. Nagaosa, Phys. Rev. B **84**, 144409 (2011).

[7] Y. Yamasaki, S. Miyasaka, Y. Kaneko, J.-P. He, T. Arima, and Y. Tokura, Phys. Rev. Lett. **96**, 207204 (2006).

[8] S. Weber, P. Lunkenheimer, R. Fichtl, J. Hemberger, V. Tsurkan, and A. Loidl, Phys. Rev. Lett. **96**, 157202 (2006).

[9] N. Mufti, A. A. Nugroho, G. R. Blake, and T. T. M. Palstra, J. Phys.: Condens. Matter **22**, 075902 (2010).

[10] K. Singh, A. Maignan, C. Simon, and C. Martin, Appl. Phys. Lett. **99**, 172903 (2011).

[11] S. H. Lee, C. Broholm, T. H. Kim, W. Ratcliff, and S. W. Cheong, Phys. Rev. Lett. **84**, 3718 (2000).

[12] A. B. Sushkov, O. Tchernyshyov, W. Ratcliff, S. W. Cheong, and H. D. Drew, Phys. Rev. Lett. **94**, 137202 (2005).

[13] J. H. Chung, M. Matsuda, S.-H. Lee, K. Kakurai, H. Ueda, T. J. Sato, H. Takagi, K. P. Hong, and S. Park, Phys. Rev. Lett. **95**, 247204 (2005).

[14] T. Rudolf, Ch. Kant, F. Mayr, J. Hemberger, V. Tsurkan, and A. Loidl, New J. Phys. **9**, 76 (2007).

[15] E. Prince, J. Appl. Phys. **32**, S68 (1961).

[16]M. Tanaka, T. Tokoro, and Y. Aiyama, J. Phys. Soc. Jpn. **21**, 262 (1966).

[17]O. Crottaz, F. Kubel, and H. Schmid, J. Mater. Chem. **7**, 143 (1997).

[18]B. J. Kennedy and Q. Zhou, J. Solid State Chem. **181**, 2227 (2008).

[19]J. M. Hastings and L. M. Corliss, Phys. Rev. **126**, 556 (1962).

[20]S. Bordács, D. Varjas, I. Kézsmárki, G. Mihály, L. Baldassarre, A. Abouelsayed, C. A. Kuntscher, K. Ohgushi, and Y. Tokura, Phys. Rev. Lett. **103**, 077205 (2009).

[21]T. Katsufuji, T. Suzuki, H. Takei, M. Shingu, K. Kato, K. Osaka, M. Takata, H. Sagayama, and T. Arima, J. Phys. Soc. Jpn. **77**, 053708 (2008).

[22]T. A. Kaplan and N. Menyuk, Philos. Mag. **87**, 3711 (2007).

[23]N. Menyuk, K. Dwight, and A. World, J. Phys. (Paris) **25**, 528 (1964).

[24]S. Funahasi, Y. Midorii, and H. R. Child, J. Appl. Phys. **61**, 4114 (1987).

[25]K. Tomiyasu, J. Fukunaga, and H. Suzuki, Phys. Rev. B **70**, 214434 (2004).

[26]K. Ohgushi, Y. Okimoto, T. Ogasawara, S. Miyasaka, and Y. Tokura, J. Phys. Soc. Jpn. **77**, 034713 (2008).

[27]G. Shirane, D. E. Cox, and S. J. Pickart, J. Appl. Phys. **35**, 954 (1964).

[28]G. L. Bacchella and M. Pinot, J. Phys. (Paris) **25**, 537 (1964).

[29]S. Klemme, H. S. C. ONeill, W. Schnelle, and E. Gmelin, Am. Mineral. **85**, 1686 (2000).

[30]H. Ishibashi and T. Yasumi, J. Magn. Magn. Mater. **310**, e610 (2007).

[31]K. Tomiyasu and I. Kagomiya, J. Phys. Soc. Jpn. **73**, 2539 (2004).

[32]E. Prince, Acta Crystallogr. **10**, 554 (1957).

[33]B. M. Wanklyn, F. R. Wondre, and W. Davison, J. Mater. Sci. **11**, 1607 (1976).

[34]High-energy spectra of MnCr_2O_4 were used to extend the reflectivity of NiCr_2O_4 above 3 eV.

[35]K. Siratori, J. Phys. Soc. Jpn. **23**, 948 (1967).

[36]S. Sugano, Y. Tanabe, and H. Kamimura, *Multiplets of Transition Metal Ions in Crystals* (Academic, New York, 1970).

[37]J. Hemberger, T. Rudolf, H.-A. Krug von Nidda, F. Mayr, A. Pimenov, V. Tsurkan, and A. Loidl, Phys. Rev. Lett. **97**, 087204 (2006).

[38]Subhro Bhattacharjee, S. Zherlitsyn, O. Chiatti, A. Sytcheva, J. Wosnitza, R. Moessner, M. E. Zhitomirsky, P. Lemmens, V. Tsurkan, and A. Loidl, Phys. Rev. B **83**, 184421 (2011).

[39]M. R. Suchomel, D. P. Shoemaker, L. Ribaud, M. C. Kemei, and R. Seshadri, Phys. Rev. B **86**, 054406 (2012).

[40]V. Kocsis *et al.* (unpublished).